

# Characterization of Teledyne Microdosimeters for Space Weather Applications

Chadwick D. Lindstrom\*<sup>a</sup>, James D. Sullivan<sup>b</sup>, Bronislaw K. Dichter<sup>c</sup>, Frederick A. Hanser<sup>c</sup>,  
Douglas Carssow<sup>a</sup>, and Gary E. Galica<sup>c</sup>

<sup>a</sup>AF Research Laboratory, Space Vehicles Directorate, 3550 Aberdeen Ave SE, Kirtland NM 87117;

<sup>b</sup>Institute for Scientific Research, 400 St. Clements Hall, Boston College;

<sup>c</sup>Assurance Technology Corporation, 84 South Street, Carlisle, MA 01741

## ABSTRACT

The Teledyne microdosimeter is a novel miniature dosimeter that has become recently available to satellite manufacturers and programs to provide awareness of the total radiation dose received by the satellite and its associated subsystems. A characterization of the response of the dosimeter to protons of energies from 30 – 200 MeV as a function of angle, energy and dose rate is presented in this paper. In addition, the response of the dosimeter to a simulated Solar proton event with several different levels of shielding has been measured. These results show that the dosimeter response is relatively uniform over a wide range of conditions for protons. Monte Carlo modeling of the dosimeter for isotropic particle fluxes (both electrons and protons) has also been accomplished. It is shown that a simplified model is appropriate in determining the response of the dosimeter when using it to design low cost, simple instruments for space weather and situational awareness applications.

**Keywords:** dosimetry, space particles, radiation detectors, total integrated dose, solar proton events

## 1. INTRODUCTION

Ideally, a space weather nowcasting system would rely on ubiquitous coverage of the near earth space environment. However, such an approach is difficult if not impossible to achieve in practice because of the extreme cost of space access as well as the large region that needs to be covered. This has long been recognized by those working on forecasting the space particle environment. Approaches relying on data assimilation using results of high-grade scientific instruments/missions or physics based models combined with data-limited miniature instruments have been proposed to address this. One possible limited-data sensor that has been recently developed is a single (hybrid) chip dosimeter that uses a conventional silicon detector to measure the total radiation dose. This microdosimeter (as named by the manufacturer Teledyne) offers the potential advantage of small size, low cost, and well-calibrated response (compared to RADFETs) that may enable easy piggybacking onto existing missions. It is, however, important that the response of this device be carefully characterized in order to use it for space particle measurements.

## 2. MONOENERGETIC PROTON BEAM MEASUREMENTS

Proton measurements were performed with nearly monoenergetic beams with energies from 30-200 MeV, incident angles of -60 to 60 degrees, and differing dose rates as indicated in table 1. The results indicate that the dosimeter performs well at obtaining a uniform response as a function of incident proton energy and angle. In addition, its dose rate response is consistent over the range of rates that were tested.

Table 1: List of run parameters during the proton test campaign

Energy Center (MeV)	Angles (Degrees)	Dose Rates (mrad-Si/s)
30	0-60, 10 degree step	4.3-6.4 (run dependent)
40	0-60, 10 degree step	3.3-4.3 (run dependent)
50	0-60, 10 degree step	0.9-11 (run dependent)
60	-60-60, 10 degree step	0.3-1 (run dependent)
80	0-60, 10 degree step	0.3-0.6 (run dependent)
200	0-60, 10 degree step	0.4-0.25 (run dependent)

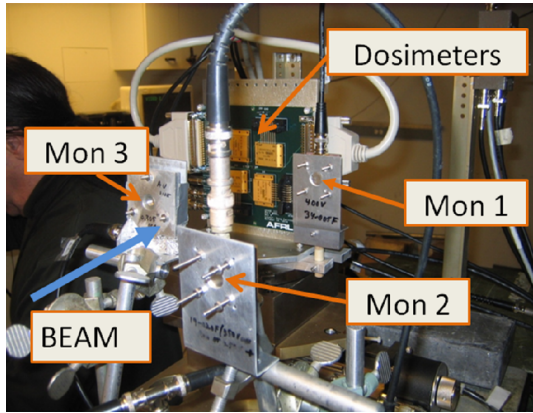
## 2.1 Experimental Setup

Four commercial grade microdosimeters were acquired from Teledyne Corporation for the proton testing. A custom printed circuit board (PCB) was designed to support the microdosimeters as well as provide connections for their power supplies and signals. The dosimeters are labeled U1 (S/N 0028), U2 (S/N 0026), U3 (S/N 0027), and U4 (S/N 0025) as shown in figure 1.

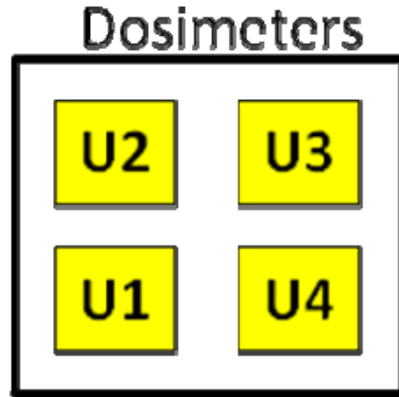
Measurements of the proton response of the microdosimeters were made March 12-13, 2011 at the Francis H. Burr Proton Therapy Center at Massachusetts General Hospital (MGH). The 230 MeV cyclotron at the facility was used to provide the proton beam for the tests. As detailed elsewhere, the proton's beam energy is changed with a combination of the energy selection system and a number of beam degraders[1]. The energy spread of this beam has been carefully measured by MGH and it behaves in fashion similar to reference 1 with  $SL2 = 10$  mm. This means that the beam spread in energy is at most 5 MeV (when the degraded beam energy is 30 MeV) and is lower for higher degraded energies. So, although the beam is not perfectly monoenergetic its spread is below 10% for energies above 40 MeV and approaches 1% at 200 MeV.

The approach taken to determine the response of the dosimeter to the proton beam is the aperture substitution method. A photograph of the test setup and a schematic illustration are shown in figure 1. The measurement process for each different proton energy as well as the solar proton event measurements used the same procedure. First the monitor 1 (Mon1) detector was placed into the center of the beam where the dosimeters will be located during data collection. At the same time, the monitor 2 (MON2) and monitor 3 (Mon3) detectors remain in their fixed location at the beams periphery. This allows determination of a scaling constant between the flux measured at Mon2 and Mon3 and the flux at the location of the dosimeters. The monitor calibration step is performed at each different beam energy and was done right before and right after the collection of data for each beam energy setting. The second step is the collection of data from the dosimeters. Here the dosimeters are placed in the beam with the center of beam placed on the center of the printed circuit board (PCB). A rotation stage with a center of rotation in the center of the pcb board was used to rotate the pcb. The dosimeters were then stepped through beam incident angles from 0 to 60 degrees and in the case of the 60 MeV beam the rotation stage was stepped through 0 to -60 degrees as well.

Standard ORTEC preamplifiers (142-B), pulse shapers (571), and single channel analyzers (551) followed by pulse counters were used to measure the flux at the monitor detectors. The discriminator threshold was adjusted so that all incoming protons were counted. The pulses were also counted using the counters of 2 UE9 Labjacks. The Labjacks digitized the 0 to 5 volt output for each channel (Low, Medium, High, and pseudo-Log) of each microdosimeter. The four microdosimeters were mounted so that each active area was near the center of the PCB. This was done to minimize the effects of any spatial inhomogeneity that may be present in the beam. In addition to this mounting strategy, a horizontal scan of the beam was taken at three different vertical positions to determine its uniformity at each energy setting. Figure 2 shows the result of a horizontal beam uniformity scan at 60 MeV. As can be seen in the figure, the beam is uniform in both the vertical and horizontal directions to within about 10% and was similarly true for the remainder of the energies that were tested.



(a)



(b)

Figure 1: (a) Picture of the experimental setup for proton beam measurements. The dosimeters and Mon1 are on a horizontal translation stage so that Mon1 can be placed in the same position in the beam as the dosimeters are during testing. Mon2 and Mon3 remain fixed throughout the testing. (b) schematic of dosimeter locations on the board

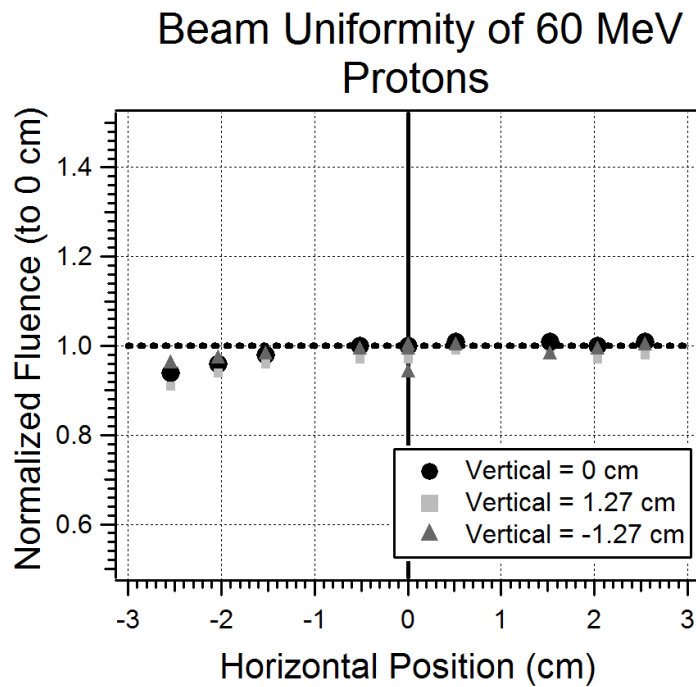


Figure 2: Beam uniformity at 3 different vertical positions as a function of horizontal position based on the Mon2/Mon1 ratio. The values are normalized to the value at (0 cm, 0 cm).

## 2.2 Data Reduction

Determination of the dosimeter response requires that an estimate of the deposited dose is obtained from knowledge of the incident proton's energy as well as the orientation, geometry, and materials in the path of the proton as it deposits energy in the detector. The approach used here is to first determine the fluence of incident protons at the location of the dosimeter using the monitor detectors. As described previously this is done using the aperture substitution method in which the fluence is first determined using the Mon1 detector at the center position of the dosimeter PCB. At the same time the Mon2 and Mon3 detectors remain at their fixed positions. At the location of Mon1 which is where the dosimeters will be; the fluence ( $F_1$ ) is simply related to the number of counts ( $N_1$ ) and the detector area ( $A_1$ ):

$$F_1 A_1 = N_1 \quad (1)$$

However, during data collection it is necessary to remove Mon1 so that the dosimeters can be placed in the beam and use Mon2 and Mon3 to estimate the flux. To do this, effective areas for Mon2 and Mon3 are defined from the measurement during this calibration step so that  $F_1$  can be determined from the number of counts measured at Mon2 and Mon3 respectively:

$$A_2^{eff} = N_2 / F_1 \quad \text{and} \quad A_3^{eff} = N_3 / F_1 \quad (2)$$

Once this calibration step is completed it then becomes possible to estimate the fluence at the dosimeters by using these effective areas and the number of measured counts at each monitor detector (Mon2 or Mon3). Using two monitor detectors one on each side of the dosimeter mounting pcb provides redundancy as well giving indications about possible spatial inhomogeneities that are developing over time.

After determining the fluence it then becomes possible to compute the estimated dose by combining this information with knowledge of the mean energy deposited per incident proton, the projected area of the detector, and the mass of the detector. The dose is given by:

$$\langle ED \rangle = \frac{\bar{E}_{dep}(\theta, E_{inc}) \cdot F_1 \cdot A_{det} \cdot \cos \theta}{\rho_{Si} \cdot t_0 \cdot A_{det}} = \frac{\bar{E}_{dep}(\theta, E_{inc}) \cdot F_1 \cdot \cos \theta}{\rho_{Si} \cdot t_0} \approx \frac{dE/dx \cdot (t_0 / \cos \theta) \cdot F_1 \cdot \cos \theta}{\rho_{Si} \cdot t_0} = \frac{1}{\rho_{Si}} \frac{dE}{dx} F_1 \quad (3)$$

where  $\bar{E}_{dep}$  is the mean energy deposited per proton;  $F_1$  is the incident fluence;  $\theta$ , is the beam incident angle;  $A_{det}$ , is the detector area in the dosimeter;  $t$ , is the detector thickness; and  $\rho_{Si}$ , is the density of silicon. A further simplification is possible as shown in equation 3 if the thickness of the detector is small relative to the proton range. The mean deposited energy can be computed in a number of ways and several ways were used including range tables [2] and the GEANT Monte Carlo code [3]. Although a Monte Carlo code is not necessary for the analysis it can be more convenient as well as enabling simulation of omnidirectional fluxes.

The error sources in the measurements can be split into two sources – statistical and systematic. For measurements that were made at MGH a minimum of 300,000 protons were collected at any energy and, thus the statistical uncertainty was less than 0.2% and was neglected in the analysis. In contrast, systematic errors associated with characterization of the test-setup will dominate. The two largest sources of error are estimating the fluence,  $F_1$ , from equation 2 and the mean energy deposited per proton. The fluence errors can come from multiple sources such as the spatial beam uniformity and the knowledge of the  $M_1$  active area. The errors associated with the energy deposited per proton are due to the beam energy spread and the accuracy of the knowledge of the beam center energy. Based on our diagnostics it is estimated that the systematic relative error is 10%.

In addition to the estimated dose, the data processing requires that the number of steps be counted. As described in Teledyne's specification sheet, the microdosimeter increments an internal 40 bit counter every time a predetermined quanta of charge appears on the internal integrator. The lower eight bits of the counter are then digitized into a 0-5 volt output for the low channel. The next eight bits (9-16) are similarly converted into a 0-5 volt analog voltage as well as bit (17-24) for the high channel. This means that the nominal voltage step is  $5 \text{ V}/256 \approx 19.5 \text{ mV}$  for each channel. This defines the microdosimeter step for the following analysis which are equivalent to 1 bit of the 40 bit counter.

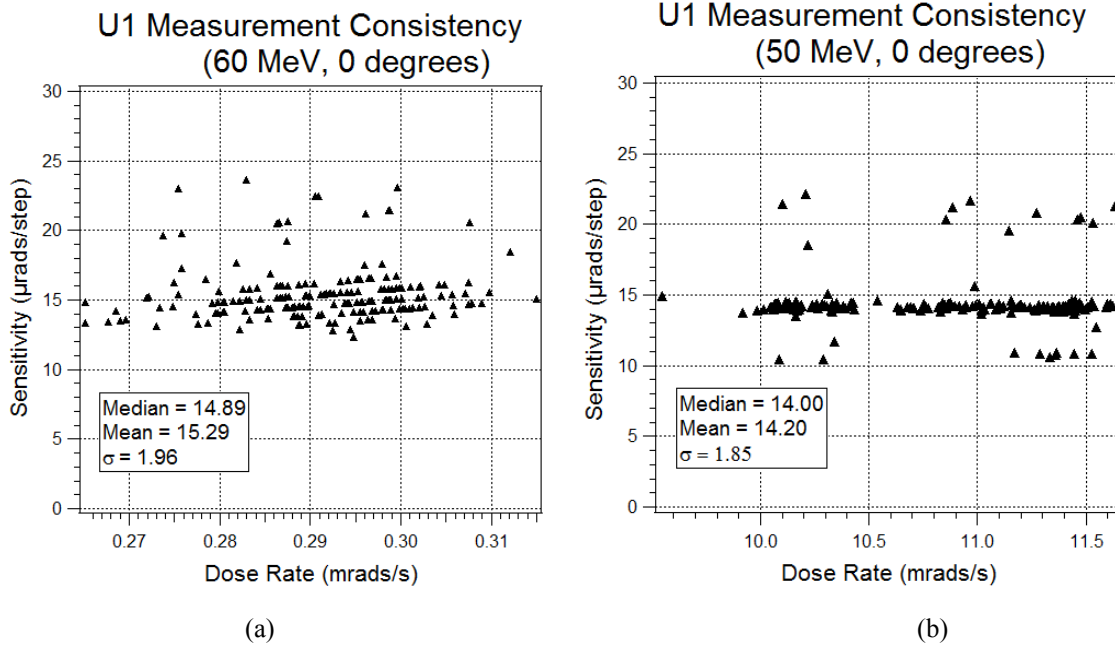


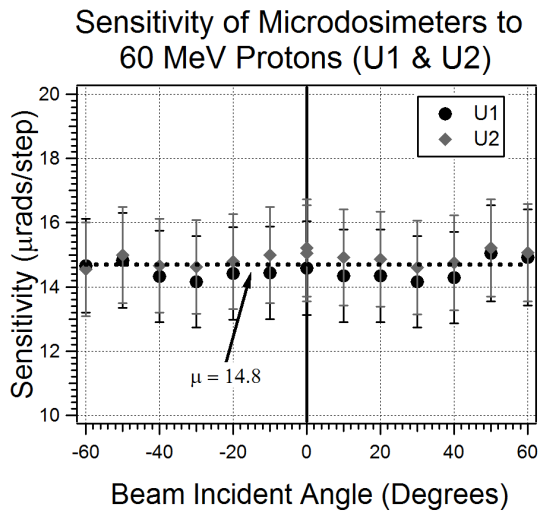
Figure 3: (a) The consistency of U1 at 60 MeV and 0 degrees (b) the consistency of U1 at 50 MeV and 0 degrees

### 2.3 Results

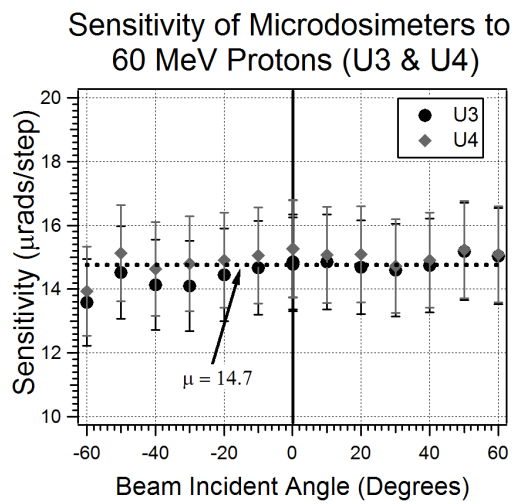
Figure 3 shows the consistency of the measurements over two different test runs. As can be seen here, the dosimeter provides consistent measurements to the level of the expected experimental errors in section 2. Figure 4 shows the angular response of the microdosimeter at 60 MeV. Because the dose per step takes into account the angular variations this should be nearly flat as can be observed here. Similar results were obtained at the other beam energies. Finally, the response of the microdosimeter at normal incidence is plotted in Figure 5. Overall the results from the beam experiments give consistent results as a function of beam energy and angle. Table 2 shows the median for each dosimeter over all measurements made in table 1 as well the standard deviation of those measurements. The median values are used in section 3 to determine the dose from a dosimeter given the number of steps it has measured.

Table 2: Median, mean, and standard deviation of all beam measurements in table 1.

Parameter	U1	U2	U3	U4
Median (µrads/step)	14.58	14.92	14.73	15.09
Mean (µrads/step)	14.78	15.09	14.84	15.11
Standard Deviation (µrads/step)	0.97	0.97	0.91	0.95

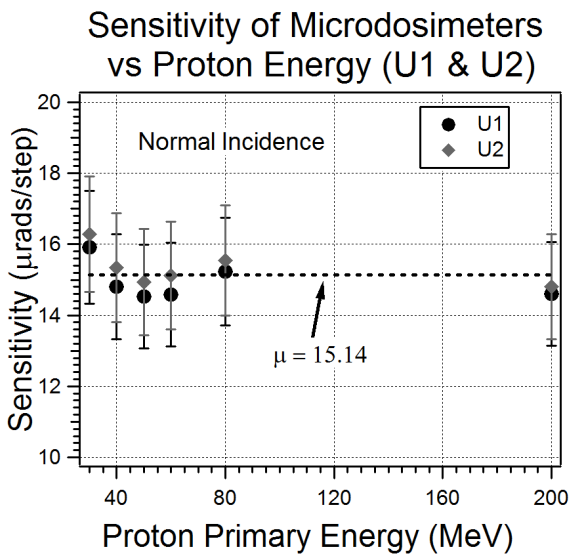


(a)

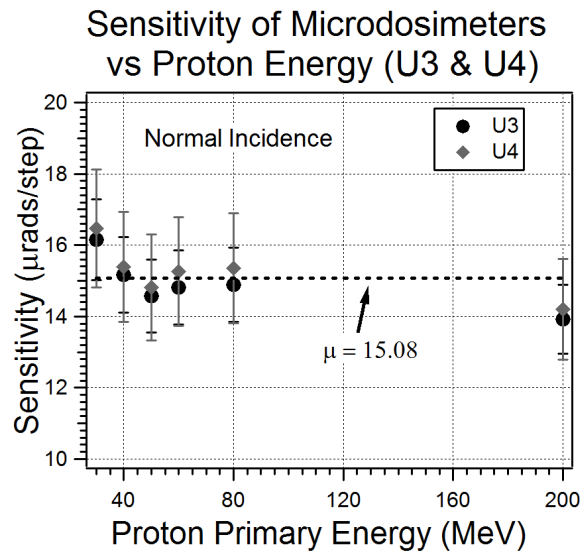


(b)

Figure 4: (a) Response of U1 and U2 as a function of incident beam angle at 60 MeV (b) response of U3 and U4 as a function of incident beam angle at 60 MeV



(a)



(b)

Figure 5: (a) Response of U1 and U2 as a function of incident proton energy (b) response of U3 and U4 as a function of incident proton energy

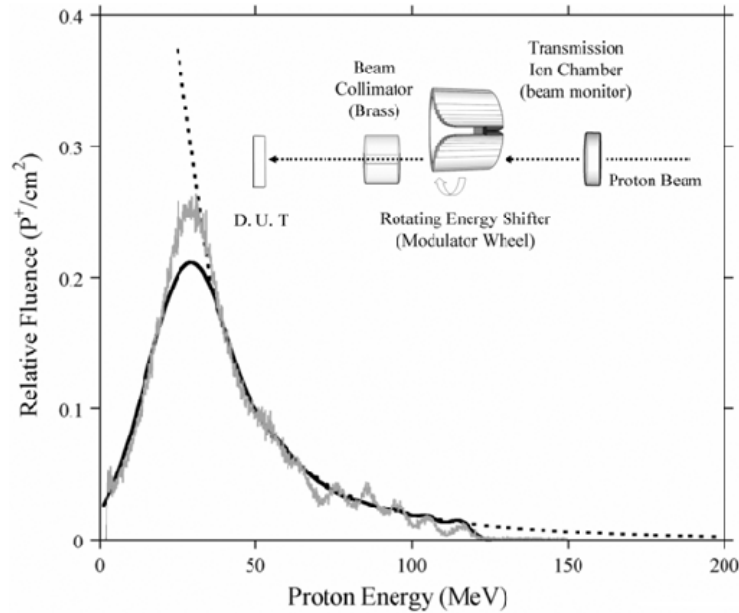


Figure 6: September 1989 solar proton event spectrum (dotted line) and MGH modulator wheel spectrum (solid black – computed, gray – measured). Figure is from reference 3.

### 3. SIMULATED SOLAR PROTON EVENT

The space particle environment is much more complex than the nominally monoenergetic beams that were used in the previous section. The three most significant differences are that the incident particle flux is a spectrum in energy, there are multiple particle species, and the flux is anisotropically distributed in angle. An experiment which could test all three cases would be extremely costly and impractical. However, MGH does provide the opportunity to test the microdosimeters with a more realistic spectrum through the use of their solar flare simulation wheel. Here this is done with the dosimeters mounted behind four different aluminum shielding thicknesses: 0 mils, 40 mils, 80 mils, and 240 mils.

#### 3.1 Experimental Setup

The experimental setup for the dosimeters as well as the monitor detectors remained the same for this experiment. A key issue that is mentioned below in the analysis section is that the thresholds on the monitor detectors are set to count every proton that is incident in them. However, as detailed in reference 3, a rotating modulator wheel was used to generate a spectrum that corresponded to the September 1989 solar proton event for energies greater than about 35 MeV [4]. The spectrum and a graphic showing the setup are reprinted from that reference for the reader's convenience in figure 6. Below about 35 MeV the spectrum deviates from the solar proton event and transitions into a nearly Gaussian spectrum at lower energies.

#### 3.2 Analysis & Results

The dose that the microdosimeters measures are compared to the estimated dose determined from the monitor detectors. The determination of the measured dose by the dosimeters is straightforward and is computed by determining the number of steps and multiplying by the appropriate median conversion factor in Table 2. Obtaining the estimated dose from the data collected by the monitor detectors is very similar to section 2. The analysis of section 2 still applies in equation 3, however, the problem becomes how to determine the mean energy deposited per proton. The mean energy deposited per proton could be easily obtained in section 2 for a single energy, however, here it is more complex. The difference is that an integral must be computed as shown in equation 5:

$$\bar{E}_{dep} = \frac{\int_0^{\infty} J(E) \cdot \bar{E}(E) \cdot f(E) dE}{\int_0^{\infty} J(E) dE} \quad (5)$$

where  $\bar{E}_{dep}$  is the mean energy deposited per proton,  $J(E)$  is the fluence ( $\#/[MeV \text{ cm}^2]$ ) as a function of incident primary energy;  $\bar{E}(E)$ , is the mean energy deposited at a particular incident proton energy (MeV), and  $f(E)$  is the fraction of the protons that penetrate the cover and reach the sensitive area of the detector and is computed through a GEANT Monte Carlo simulation. Table 3 shows that the results agree to within 9% which is within the margin of error of the experiment, and suggests that the dosimeter can accurately measure total dose by proton energy distributions that are similar to the space environment.

Table 3: Dosimeter measurements of the simulated solar proton spectrum

Dosimeter	Al Shield (mils)	Nominal $E_{threshold}$ (MeV)	Estimated Dose from Mon 1 & 2 (mrads)	Dosimeter Measured Dose (mrads)
U1	0	9.5	935	856
U2	0	9.5	935	865
U3	0	9.5	935	867
U4	0	9.5	935	868
U1	40	17	806	806
U2	40	17	806	806
U3	40	17	806	803
U4	40	17	806	813
U1	80	23	630	675
U2	80	23	630	678
U3	80	23	630	670
U4	80	23	630	683
U1	240	38	301	289
U2	240	38	301	290
U3	240	38	301	287
U4	240	38	301	295

#### 4. MONTE CARLO SIMULATIONS

All the previous analysis focused on unidirectional beam measurements, however, the space environment is more complex because the particles come from all directions that can cause dose. In addition, it is necessary to account for multiple particle species: in particular electrons and protons. As mentioned previously, this is difficult to account for in experiments. Here Monte Carlo calculations are often the best approach. In the case of the microdosimeter, an important issue is that the full geometry is not available due to proprietary restrictions of the data. However, AFRL has worked out an agreement that allowed us to compute the response of the dosimeter for the full geometry (including the proprietary details) and then compare this to a reduced geometry version that is not proprietary. The response functions shown here are for an isotropic flux that is impacting the dosimeter from all sides.

The response function of the dosimeter is slightly different than the computations that have been presented above since the flux is incident from all sides on the dosimeter. Here it is useful to introduce the geometric factor which is the ratio between the incident isotropic fluence and the number of counts (i.e. protons) [5]. Since the dosimeter measures dose (i.e. rads) the number of protons that ultimately are counted must be multiplied by the mean energy deposited per proton that strikes the detector. This implies the following definition of the response function:

$$D = \frac{1}{m_{\text{det}}} \int_0^{\infty} \bar{E}(E)G(E)j(E)dE = \int_0^{\infty} R(E)J(E)dE \rightarrow R(E) = \frac{G(E)\bar{E}(E)}{m_{\text{det}}} \quad (6)$$

where  $\bar{E}(E)$  is the average energy deposited in the detector summed over all incident angles,  $G(E)$  is the geometric factor ( $\text{cm}^2 \text{sr}$ ),  $J(E)$  is the differential isotropic fluence ( $\#/\text{cm}^2 \text{sr MeV}$ ),  $D$  is the dose (rads),  $m_{\text{det}}$  is the detector mass, and  $R(E)$  is the response (rads  $\text{cm}^2 \text{sr}$ ). Although the response function is not the only way to model the measured dose, it is useful in performing spectral inversion by fitting typical spectral shapes (such as a power law) to estimate the particle spectrum.

The simplified dosimeter model is shown in figure 7. It has been taken from the description of the microdosimeter's data sheet. It consists of the detector in its approximate position in the lower left corner. The dimensions and materials of this model are given in table 4. Figure 8 shows the response functions for both electrons and protons from the reduced geometry model shown in figure 7 on a log-log scale and also compare this model with the more detailed geometry model. The high frequency variation is due to the statistical nature of the Monte Carlo technique. It is clear that the simplified model is sufficient to capture the response of the dosimeter.

The response functions have jumps at energies where the protons and electrons start to penetrate the side and bottoms of the dosimeter. For the case of a surface mounted dosimeter with the bulk of the spacecraft behind it, it is anticipated that most of the dose will be contributed through the front surface. However, for a dosimeter mounted deep within the spacecraft that is surrounded on all sides by material that is much thicker than the sides the penetrating particles will most likely see the whole geometric factor of the detector. Even then the effect is only a factor of 2-3 which may not be critical in applications requiring just situational awareness. However, for modeling of the space environment and its effects this is something that may need to be taken into account.

Table 4: Pertinent Dimensions of simplified model

	Height (cm)	Width (cm)	Length (cm)	X (cm)	Y (cm)	Z (top = 0) (cm)	Material
Top	0.0254	2.54	2.54	N/A	N/A	0	Kovar*
Bottom	0.1016	2.54	2.54	N/A	N/A	0.3429	Kovar
Sides	0.3429	0.1016	2.54	N/A	N/A	N/A	Kovar
Detector	0.025	0.3	0.7	0.208	0.2469	0.2667	Silicon
Detector Mount	0.0635	0.6	0.76	0.1953	0.2169	0.2921	Lavite**

\* Kovar is 54% Fe, 29% Ni, 17% Co, 0.3% Mn, 0.2% Si, <0.01% C with a density 8.35  $\text{g}/\text{cm}^3$

\*\* Lavite is  $\text{Al}_6\text{O}_{13}\text{Si}_2$  and has a density of 2.3  $\text{g}/\text{cm}^3$

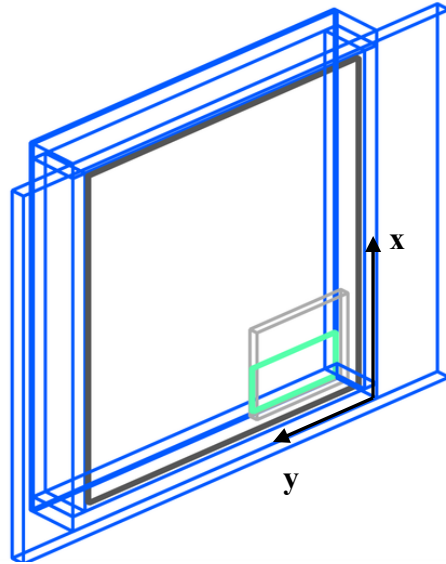


Figure 7: The simplified chip dosimeter as modeled in GEANT. The blue lines outline the case, the light grey the detector mount, and the green is the Si detector

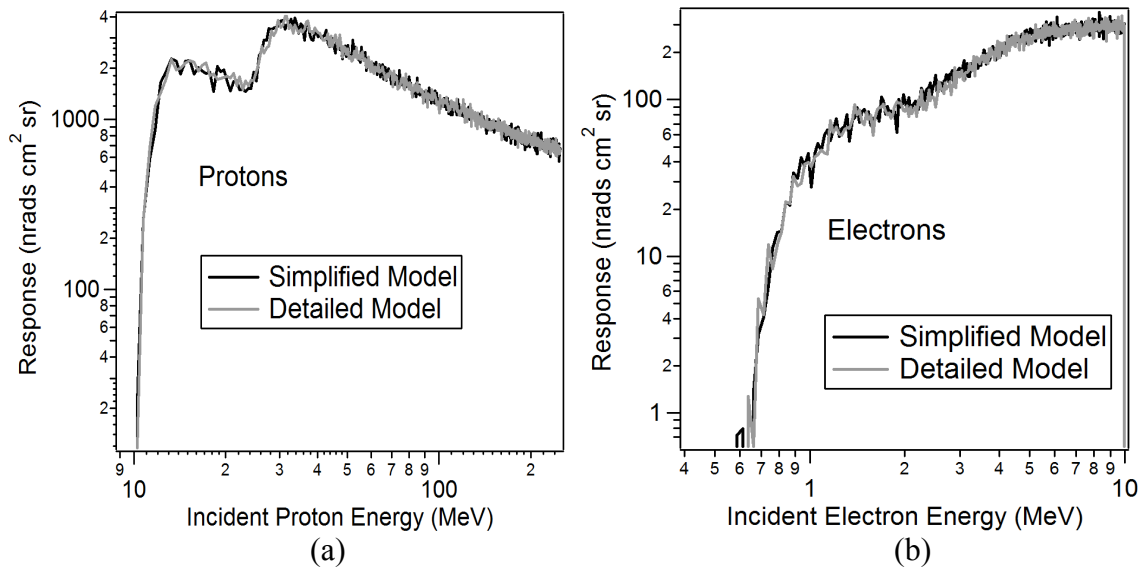


Figure 8: (a) The response functions for protons (b) The response functions for electrons

## 5. CONCLUSION

The Teledyne microdosimeter demonstrated that its dose response to protons is consistent over a wide range of energy, angles, and dose rates for nominally monoenergetic beams. In addition, it also shown that it gives a response to a simulated proton spectrum that is in good agreement with the response for monoenergetic beams. Finally, a simplified internal geometry model of the dosimeter has been presented that can be used for instrument modeling purposes. The microdosimeter shows good promise for a low cost, low impact instrument that can be used to measure the space particle environment and give insight into how space environment is affecting a space vehicle.

## REFERENCES

- [1] Cascio, E. W., Sisterson, J. M., Gottschalk, B., et al., "Measurements of the Energy Spectrum of Degraded Proton Beams at NPTC", Proc. of 2004 IEEE Radiation Effects Data Workshop, 151-155 (2004).
- [2] Janni, J. F., "Calculation of energy loss, range, pathlength, straggling, multiple scattering, and probability of inelastic nuclear collisions for 0.1 to 1000 MeV protons", Air Force Weapons Laboratory Technical Report AFWL-TS-65-150, 1 (1966).
- [3] Agostinelli, S., and et al., "Geant4: A simulation toolkit," Nucl. Instrum. Meth. A. vol. 506(3), 250-303 (2003).
- [4] Cascio, E. W., "A Solar Flare Simulation Wheel for the Radiation Test Beamline at the Francis H. Burr Proton Therapy Center," IEEE Transactions on Nuclear Science, 55(6), 3428-3434 (2008).
- [5] Sullivan, J. D., "Geometrical Factor and Directional Response of Single and Multi-Element Particle Telescopes," Nuclear Instruments and Methods, 95(5), 5-11 (1971).